World Journal of Nuclear Science and Technology, 2016, 6, 261-283
http://www.scirp.org/journal/wjnst
ISSN Online: 2161-6809
ISSN Print: 2161-6795

Improvement of Beam Energy Measurement System for BES-III

Jianyong Zhang[1], Xiao Cai[1], Xiaohu Mo[1], Muchnoi Nickolai[2], Achasov Mikhail[2], Elena Abakumova[2], Harris Fred[3]

[1]Institute of High Energy Physics, CAS, Beijing, China
[2]Budker Institute of Nuclear Physics, Siberian Branch of the Russian Academy of Sciences, Novosibirsk, Russia
[3]University of Hawaii, Honolulu, USA
Email: jyzhang@mail.ihep.ac.cn, moxh@mail.ihep.ac.cn

How to cite this paper: Zhang, J.Y., Cai, X., Mo, X.H., Nickolai, M., Mikhail, A., Abakumova, E. and Fred, H. (2016) Improvement of Beam Energy Measurement System for BES-III. *World Journal of Nuclear Science and Technology*, **6**, 261-283.
http://dx.doi.org/10.4236/wjnst.2016.64025

Received: September 2, 2016
Accepted: October 11, 2016
Published: October 14, 2016

Abstract

The beam energy measurement system is significant and profit for both BES-III detector and BEPC-II accelerator. The detection of the high energy scattering photons is realized by virtue of the Compton backscattering principle. Many advanced techniques and precise instruments are employed to acquire the highly accurate measurement of positron/electron beam energy. During five years' running period, in order to satisfy the requirement of data taking and enhance the capacity of measurement itself, the upgradation of system is continued, which involves the components reformation of laser and optics subsystem, replacement of view-port of the laser to vacuum insertion subsystem, the usage of electric cooling system for high purity germanium detector, and the refinement of data acquisition and processing subsystem. The upgrading of system guarantees the smooth and effective measuring of beam energy at BEPC-II and accommodates the accurate offline energy values for further physics analysis at BES-III.

Keywords

Laser, HPGe Detector, Beam Energy Measurement

1. Introduction

The upgraded Beijing electron-positron collider (BEPC-II) is a τ-charm factory with a beam energy ranging from 1.0 to 2.3 GeV and the design peak luminosity of 10^{33} $cm^{-2}\cdot s^{-1}$ [1] [2] at 1.89 GeV, which was achieved at the evening of April 5, 2016. The upgraded Beijing spectrometer detector (BES-III) with high efficiency and good resolution for both charged and neutral particles was constructed and started data taking in 2008 [3]

[4]. A large amount of data are obtained and analyzed, the statistical uncertainties in physics analysis become smaller and smaller, at the same time the systematic uncertainties play more and more prominent roles [5]-[7], one of which is the uncertainty due to the measurement of beam energy. To decrease such an uncertainty, starting from year 2007, a high accuracy beam energy measurement system (BEMS) located at the north crossing point (NCP) of BEPC-II was designed, constructed, and put into the commissioning at the end of 2010 [8]-[11]. The launching of system was excellently well, two days were utilized to perform the ψ' scan. The mass difference between the PDG 2010 value and the measured result by BEMS is 1 ± 36 keV, the deviation of which indicates that the relative accuracy of BEMS is at the level of 2×10^{-5} [10].

The establishment of BEMS improves the measurement capacity of both accelerator and detector, and BEMS can provide the beam energy, energy spread and their corresponding errors, all of which are crucial and useful information for the physical analysis of BES-III and the luminosity tuning at BEPC-II. The first exhibition of such a capacity of BEMS is the test scan of τ mass, which was performed at the end of 2011. The integrated luminosity of τ sample was 23.26 pb^{-1}, the mass of τ lepton was determined as $m_\tau = 1776.91 \pm 0.12^{+0.10}_{-0.13}$ MeV [12], among which the systematic uncertainty due to energy scale is less than 0.09 MeV.

During five years' running, BEMS had participated various data collections at BES-III, including J/ψ and ψ' resonance samples, R value scan samples, the high excited charmonium states samples and so forth. The high precision beam energy values were measured and accommodated for the offline data analysis. **Figure 1** shows the measured results of BEMS during the data taking of J/ψ resonance. The fluctuation of energy is obvious. This is the first time to display the energy variation status of BEPC-II with such a high accuracy.

The high precision of energy calibration acquired by BEMS is based on Compton backscattering principle. The working scheme of this system can be depict briefly as follows [13]: firstly, a laser source provides a laser beam, and an optics system focuses the laser beam and guides it to make head-on collisions with the electron (or positron) beam in the vacuum pipe, where the Compton backscattering process happens; after that, the backscattering high energy photon will be detected by a High Purity Germanium (HPGe) detector. More engineering details can be found in Ref. [10]. In fact, many advanced techniques and precise instruments are employed to achieve such a highly accurate measurement of beam energy. The whole system can be sub-divided into four parts according to their technique and engineering characters: 1) laser source and optics system, which supplies low energy laser and focused photons; 2) laser to vacuum insertion system, where a laser beam collides with electron or positron beam; 3) HPGe detector to measure backscattering high energy photons; 4) data acquisition and running control system for information processing and analyzing. The layout schematic of the system is shown in **Figure 2**.

In order to satisfy the physics requirement, and increase the accuracy of measurement, improvements for BEMS have been performing since its commissioning. The

details are described in the following sections. The laser and optical system upgrade is introduced in Section 2. The improvement of laser to vacuum insertion system is presented in Section 3. The update of detection system is introduced in Section 4. The data acquisition and process system is presented in Section 5. The interlock system is introduced in the Section 6. The upgrade effect is shown in Section 7. Finally, there is a short summary.

2. Laser and Optical System

This system is composed of a laser source to supply low energy photons, two lenses to focus the beam light, and three reflecting mirrors and one movable prim to direct the laser beam into the storage ring tunnel. All relevant instruments are installed along the shielding concrete wall as shown in Figure 2. The upgrade processes are described chronologically below.

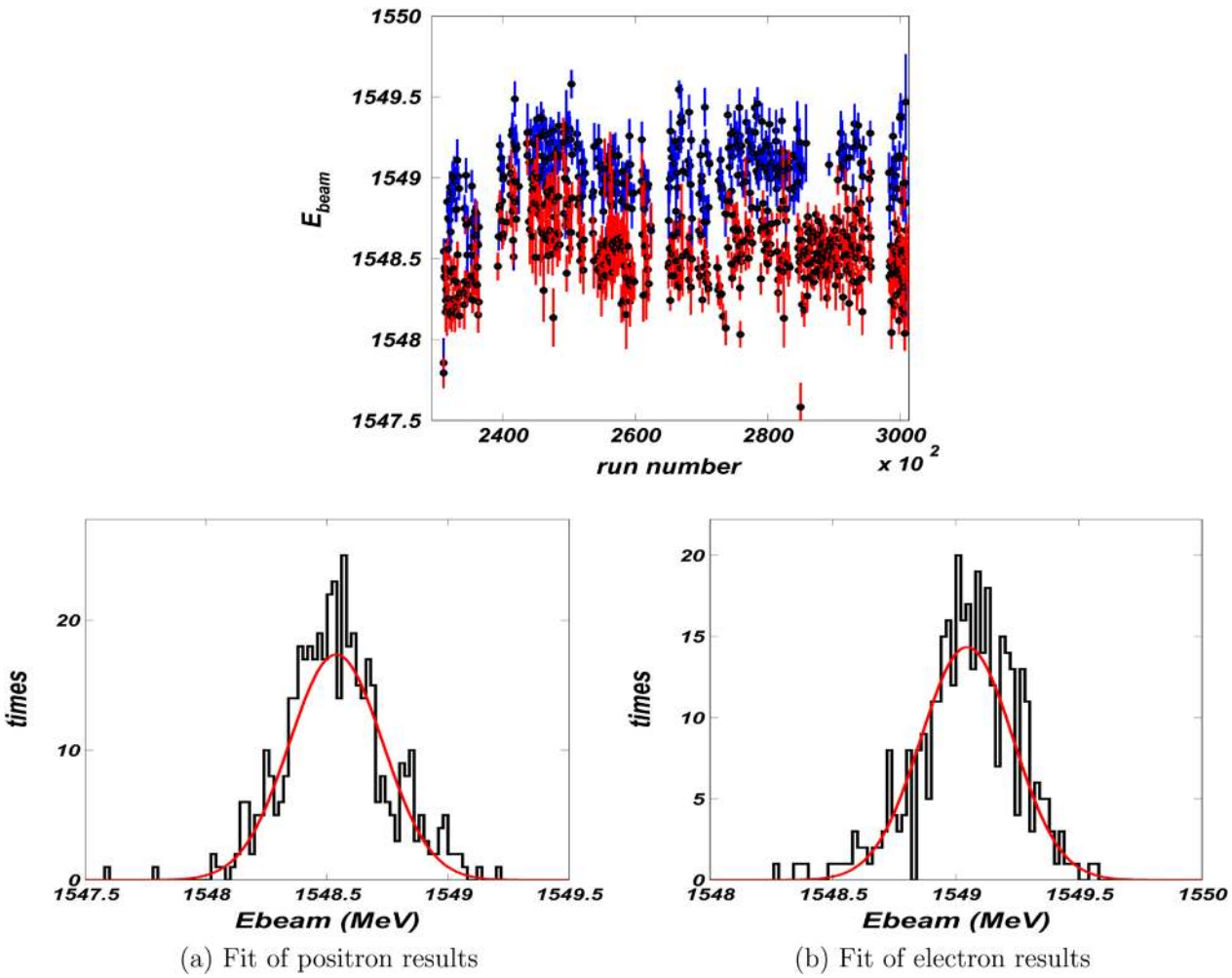

(a) Fit of positron results (b) Fit of electron results

Figure 1. Beam energy measurement results during the J/ψ data taking. The horizontal coordinate is the running number; the points with blue error bar are results for electron beam, while the points with red error bar are for positron beam. The averaged energy values for electron and positron beams are respectively 1549.0 ± 0.2 MeV and 1548.5 ± 0.2 MeV, with corresponding deviations of 0.20 ± 0.01 and 0.19 ± 0.01 MeV.

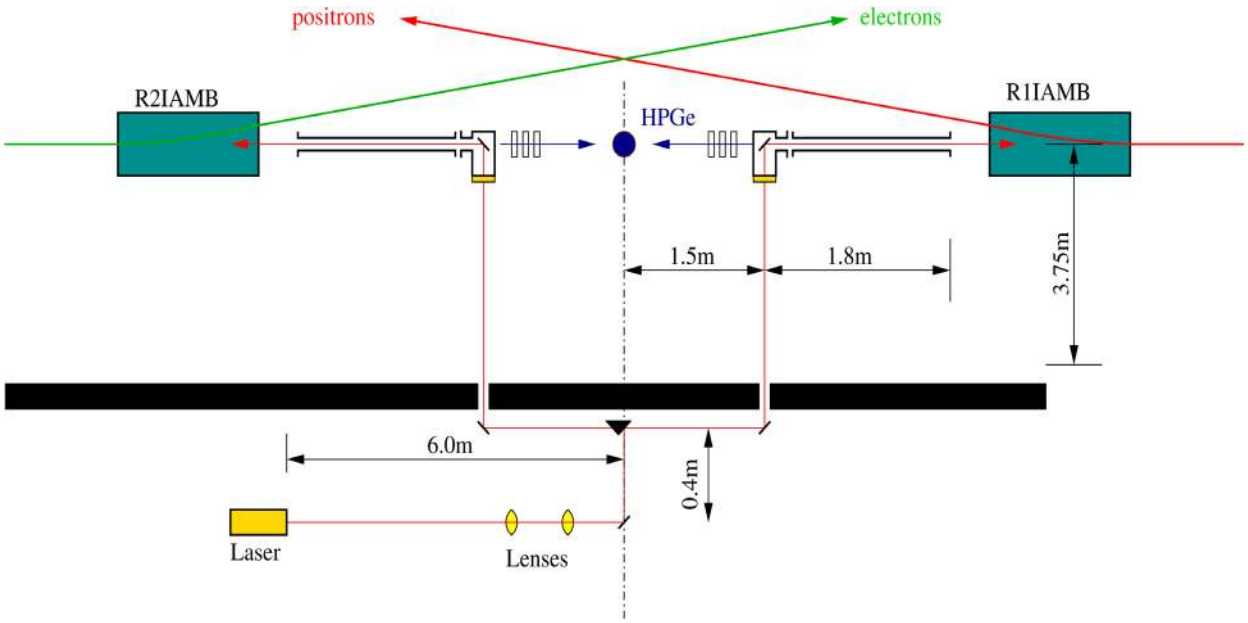

Figure 2. Simplified schematic of beam energy measurement system. The positron and electron beams are indicated. R1IAMB and R2IAMB are accelerator magnets, and the HPGe detector is represented by the dot at the center. The shielding wall of the beam tunnel is shown cross-hatched, and the laser is located outside the tunnel.

2.1. Lenses Update

The laser beam is focused at the BEPC-II vacuum chamber entrance flange, where the geometrical aperture is minimal: vertical size × horizontal size is 14 mm × 50 mm. Since the total distance from the laser output aperture to the entrance flange of the BEPC-II vacuum chamber is about 18 m, the focusing function can hardly be realized by a single lens, but two lenses.

Previously, a doublet of zinc selenide (ZnSe) lenses with focal lengths of 40 cm was placed respectively at distance of 300.0 and 381.6 cm far from the laser output window. They provided the laser beam transverse size at the flange from 2.0 to 2.5 mm for collision. The laser transmissivity for the two lenses were 69% and 61% respectively. The synthetic transmissivity is merely 42%, which means more than half photons were consumed during the focusing.

Two new ZnSe lenses were manufactured. The focal length of the two lenses is 42 cm, and they are placed at 330 cm and 415 cm in front of the laser output window separately for the laser focusing. The transmissivity to laser is 99% for each lens, which tends to guide most of photons into the vacuum pipe to collide with the electron or positron beams. Comparing with the old lenses system, the new one greatly suppresses the waste of photons.

2.2. Prism Replacement

During the operation of BEMS, the energy of positron beam or electron beam is measured alternately. The alternation is executed by a translatory reflector prism, as shown in Figure 3, where (a) and (b) are a schematic explanation for beam path selection, and

(c) is a physical picture of translatory prism. The laser beam is directed by the prism towards the right or left mirror to collide with the positron or electron beam automatically. During several years' running, dusts accumulated in the groove of prism support produce a braking effect on the automatical movement and eventually lead to the immobilization of prism. Finally, the switch between electron and positron has to be manipulated manually, which is actually intolerable for full-day continuous measurement.

Instead of changing the old prism with a new one, a brand new design is put forth to prevent recurrence of the similar problem. A rotary platform shown in Figure 4(a) is

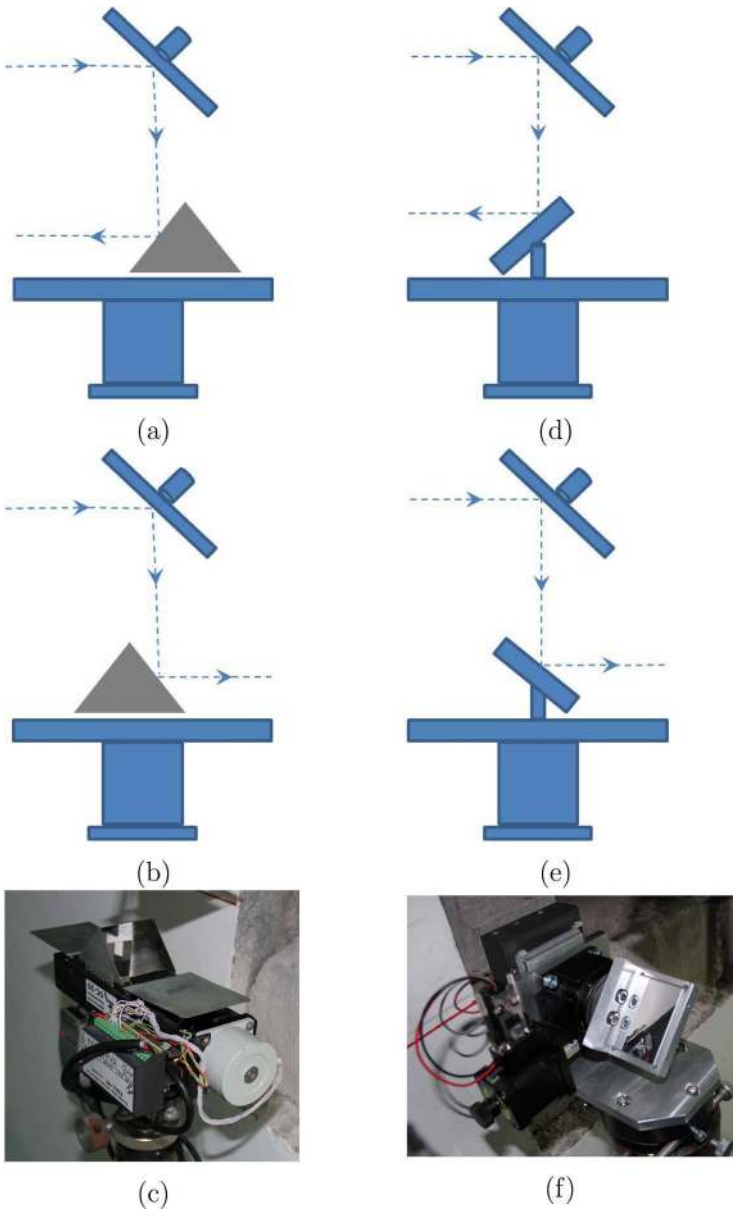

Figure 3. The left side is the translatory prism and the right side is the rotary platform. The laser light, represented by the dash line, is reflected to the electron ((a), (d)) and positron ((b), (e)) side using translatory prism and rotary platform respectively. The assembly pictures of translatory prism and rotary platform are shown in (c) and (f) separately.

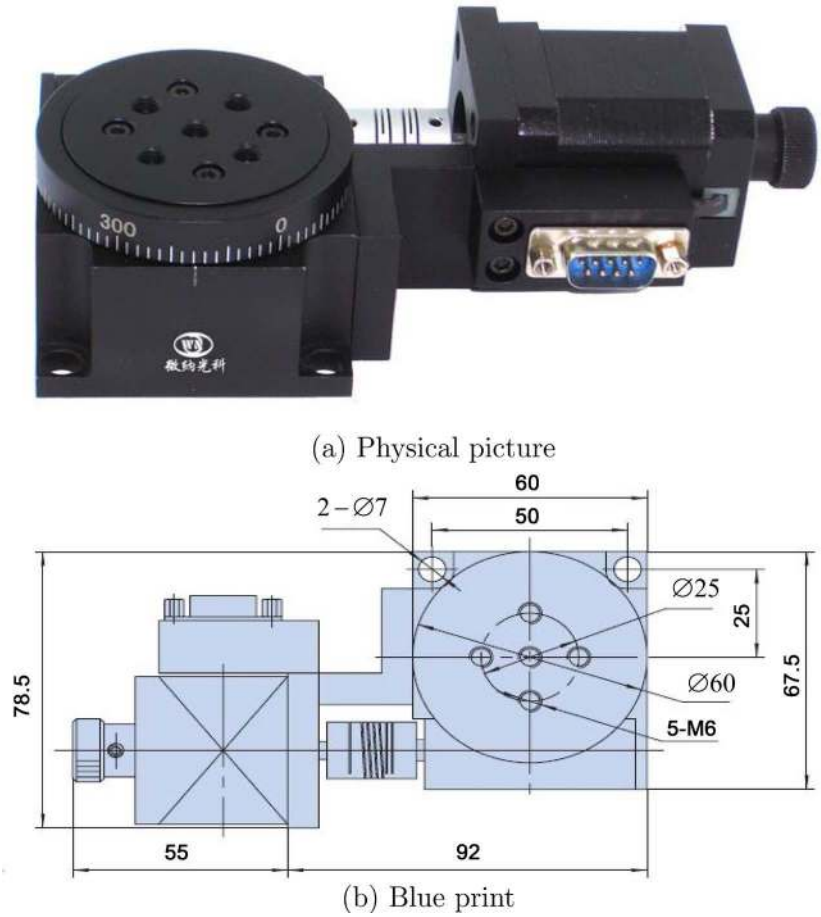

Figure 4. The rotary platform stage adopted by BEMS. (a) shows the physical picture of the rotary platform, which is connected with the step controller by RS232 cable. (b) shows the blue print of the rotary platform where the detailed dimensions are presented.

investigated. The rotary gear is covered below the platform to ensure durable. A through hole at the center of the rotary platform satisfies the coaxial requirement strictly with the center of rotation, clearly in **Figure 4(b)**. The center aperture of the rotary platform suffices the strict tolerance limitation, both of which will be benefit to the precise positioning. The absolute positioning accuracy of the rotary platform is 0.005 degree. A special support was designed, forged, and installed to fix the rotary platform. A mirror with its frame was fixed on the rotary platform to change the direction of the laser. The rotary platform is controlled by a step motor, whose step is 1.5×10^{-6} rad. The rotation angle of the mirror is controlled precisely, so that the laser will be reflected to the right or left to make collision with positron or electron beam.

Figure 3(d) and **Figure 3(e)** are the schematic explanation for beam path selection by rotary mirror, and (f) is the assembly picture of the rotary platform after installation.

2.3. Laser Improvement

The laser source of initial photons is produced by the GEM Selected 50™ CO_2 laser from Coherent, *Inc.* It is a continuous operation (CW), high power, and single-line

narrow-width laser. It provides 25 W of CW power at the wavelength $\lambda_0 = 10.835231\,\mu m$ (γ-quantum energy $\omega_0 = 0.114426901\,eV$), which corresponds to 10P42 transition in the carbon dioxide molecule [14]. The relative accuracy of ω_0 is better than 0.1 ppm.

After five years' running, the grating coat became too thin, and the number of photons produced by the laser became so rare that the scattering photons after collision were too weak to be detected. The laser had to be returned to the manufactory for repairing. Considering the designed beam current of BEPC-II is 910 mA, the requested physics energy region (1.0 - 2.3 GeV) is wide, and the background near the NCP is complicated, a more powerful laser is needed. Therefore, a more powerful laser with output power up to 50 W was chosen as the laser source. The wavelength of the new laser is of $\lambda_0 = 10.591035\,\mu m$ (γ-quantum energy $\omega_0 = 0.117065228\,eV$), which corresponds to 10P20 transition in the carbon dioxide molecule [14].

The power of the new laser is about twice that of the old one, so that more laser photons are gathered at the interaction region and collide with the beam. Therefore, the Compton edge will be easier to form, or the data taken time for measurement will be shortened.

3. Laser to Vacuum Insertion System

The laser to vacuum insertion system is a crucial part of BEMS [15]. As shown in **Figure 5**, the system consists of a special stainless vacuum chamber with entrance viewport and a reflect copper mirror. From this part, the laser beam is inserted into the vacuum chamber, reflected 90 degrees by the copper mirror and makes the head-on collision with the positron or electron beam. Then the back-scattered photons pass through the copper mirror and are detected by the HPGe detector. Since the mirror is heated by reflecting laser and synchrotron light, it must be cooled by cooling water. In addition, since this part connects with the beam pipe of the storage ring, after installation, the vacuum chamber must be baked at 250 degree for twenty four hours in order to ensure that the vacuum pressure must be better than 2×10^{-10} Torr.

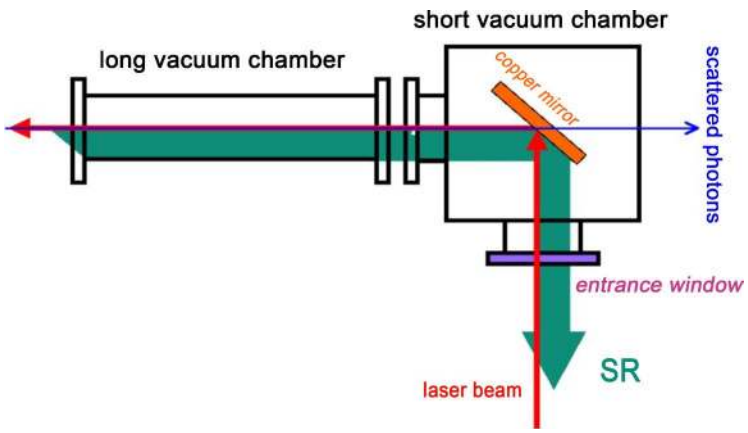

Figure 5. Schematic diagram of the laser to vacuum insertion of BEMS. SR represents the Synchrotron Radiation light.

Two advanced techniques are adopted at the laser to vacuum insertion system, and the first one is the synchrotron light alignment technique. As shown in Figure 2, it can be noted that the beam of positron or electron is bent at the NCP. The collision between laser and beam happens just before the bend, which avoids the interference of beam current with backscattering photons. At the same time, the synchrotron light radiates along the tangent direction of the bent beam and the path of this synchrotron light is the same path as that of the laser beam but in the opposite direction (refer to Figure 5). Therefore, the synchrotron light can be used to pin down the laser beam alignment. The actual process of light path adjustment is as follows.

The copper mirror is mounted on a special copper support, which can be tuned by bending the vacuum flexible bellow using screwdriver. The back penal of the copper support is shown schematically in Figure 6(a), where the positions of four screws are

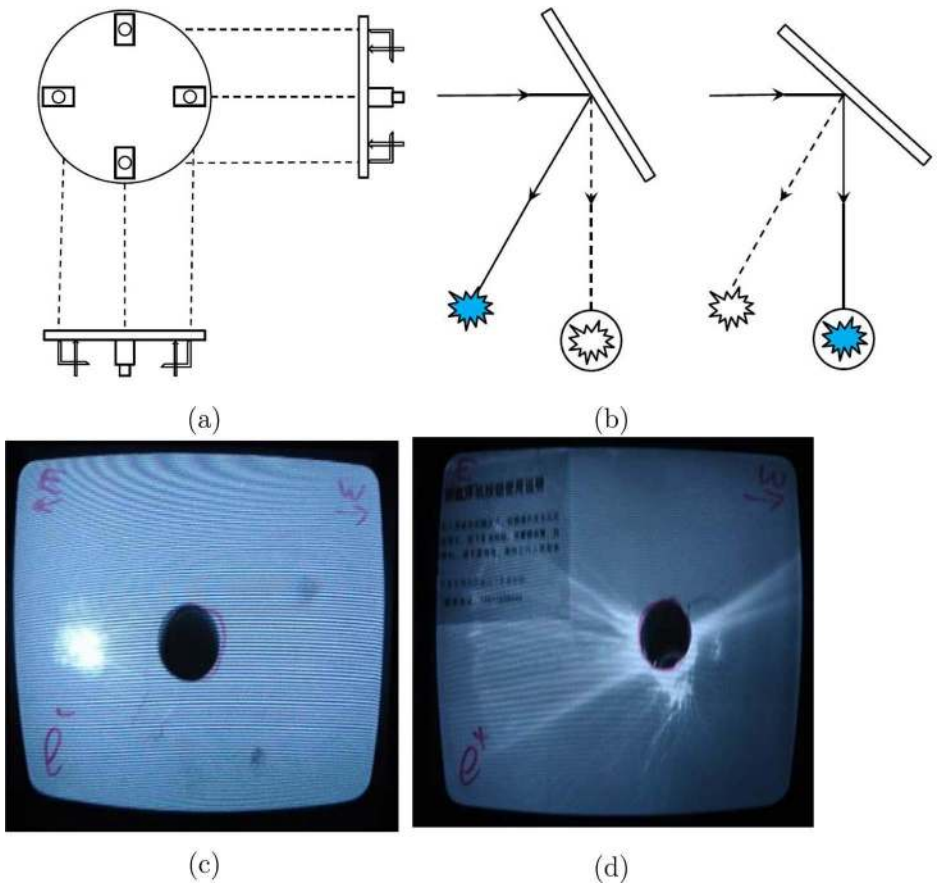

Figure 6. (a) The copper mirror mounted on a special support by screws, the adjustment for horizontal direction and vertical direction are separated. (b) The simplified schematic of tuning the optical path. The solid and dashed line indicates the light path before and after (after and before) tuning. The circles mean the holes in the shielding wall in the BEPCII tunnel. By means of adjusting the direction of mirror, the light was moving into the holes in the wall. (c) and (d) are the effect of the copper mirror adjustment using cameras. The white spots are the synchrotron radiation and the black circles are the holes of wall in BEPCII tunnel. (c) Before the copper mirror adjustment, the synchrotron light is reflected on the wall. (d) After the mirror adjustment (b), the synchrotron light is reflected into the holes of the wall.

denoted. The adjustment for the horizontal and the vertical directions are realized by two pairs of screws separately. The adjustment distance l can be calculated as follows when the screw rotates one circle:

$$\frac{d}{D}=\frac{l}{L}. \tag{1}$$

where $d=0.5$ mm is the one circle distance for the screw; D is the dimension of the support, which is 70 mm for the vertical support, and 39 mm for the horizontal one; $L=4150$ mm is the distance between the copper mirror and the hole in the wall. During the running period of BEPC-II, the synchrotron light spots are visible. Two cameras are installed in front of the holes in the tunnel wall, the east for the positrons and the west for electrons. The distance between the spot and the center of the hole is recorded. Comparing with the one circle distance obtained using Equation (1), the number of turns can be evaluated, the optical path would be adjusted accordingly. Two pairs of screws accommodate two dimensional adjustment of light path. The cartoon drawn in **Figure 6(b)** shows schematically the tuning of the optical path. Usually tuning one or two times is enough. The actual adjustment effects are displayed in **Figure 6(c)** and **Figure 6(d)** by means of the cameras. It is clear that after the mirror adjustment, the synchrotron light passes through into the holes in the wall and is reflected to where the laser will pass. Similarly, the laser can be transferred through the hole and reflected into the vacuum pipe to make collision with the beam.

The second advanced technique employed in this part is the manufacture of the viewport. As shown in **Figure 5**, the entrance viewport is pivotal for the laser to vacuum insertion system, since it is in charge of the light path adjustment and the laser beam insertion. The viewport must be transparent to both laser beam and synchrotron light. Two types of entrance viewports [16] [17] were sequentially used by BEMS, one was based on gallium arsenide (GaAs) monocrystal plate and the other was zinc selenide (ZnSe) polycrystal plate.

At the beginning, a GaAs plate with diameter of 50.8 mm and thickness of 3 mm was adopted by BEMS. However, the GaAs crystal is not transparent for the visible light, it transmits infrared radiation. In order to detect the spots of infrared light, IR-sensitive video cameras were used. During the BEMS running, the GaAs viewport was changed three times to improve the transmissivity of the window. At last a ZnSe plate with thickness of 8 mm was adopted. The laser transmission rate rose up from 60% to 76%. In addition, more visible synchrotron light is transparent, which is convenient for the optical path adjustment.

4. HPGe Detection System

As aforementioned in the working scheme, the backscattering high energy photons will be detected by a HPGe detector, which is a key instrument of BEMS. The accuracy of beam energy depends solely on the detection results of the HPGe detector. There are two crucial conditions for HPGe detector functioning properly and enduringly for BEMS at BEPC-II, that is low temperature and radiation protection. The upgrades

about these two aspects are narrated below.

4.1. Cryogenic System Upgrade

4.1.1. HPGe Detector

The purpose of an HPGe detector is to convert gamma rays into electrical impulses which can be used with suitable signal processing, to determine their energy and intensity. An HPGe detector is a large germanium diode of the p-n or p-i-n type operated in the reverse bias mode. At a suitable operating temperature (normally ≃ 85 K), the barrier created at the junction reduces the leakage current to acceptably low values. Thus an electric field can be applied that is sufficient to collect the charge carriers liberated by the ionizing radiation.

There are two kinds of HPGe detectors, n-type and p-type. Adopted by BEMS is the p-type coaxial detector manufactured by ORTEC (model GEM25P4-70), whose energy resolution for the 1.33 MeV peak of ^{60}Co is 1.74 keV (FWHM), with the relative efficiency is 25%. The detector is connected to the multichannel analyzer of ORTEC DSpec Pro (MCA), which transfers data using the USB port of the computer.

4.1.2. Two Cryogenic Systems

Low temperature is critical for HPGe detector functioning properly [18]. Two approaches are usually employed to get the temperature below 100 kelvins (K): liquid nitrogen (LN_2) and electric coolers [19] [20]. The former was firstly utilized for cooling the HPGe detector at BEMS. The germanium crystal, with diameter of 57.8 mm and height of 52.7 mm, was cooled down to the working temperature by connecting with the thermal transfer device, the cryostat and the extension rod that dipped into the LN_2-full dewar, and the cold was conducted from the dewar to the germanium crystal.

One common LN_2 filling method, namely self-pressurizing technique, was used by BEMS. The filling procedure is shown in **Figure 7(a)**, more details can be found in Ref. [21]. During the data taking period of BES-III, the BEMS is kept running simultaneously. The LN_2 has to be supplied once a week to avoid unexpected warm-ups of HPGe detector. However, such a regular filling schedule is unfavorable by both BES-III detector and BEPC-II accelerator. To the detector, some precious data taking time has to be consumed for refilling LN_2; to the accelerator, some time has to used to recover the preceding good running status.

From the point view of continuous cooling, an electric cooler is an ideal replacement for the LN_2. An electric cooler, composed of a compressor, transfer hose, heat exchanger, and cold head, was adopted for HPGe detector. All parts except for the heat exchanger are visible to user, as shown in **Figure 7(b)**. The only concern here is the continuous electricity power. So that an uninterruptible power system (UPS) is used for the cooler, which guarantees the most safe power supply.

4.1.3. Resolution Comparison of Two Cryogenic Systems

In fact, the electric cooler was once the first choice of BEMS, but the resolution of HPGe under the two cryogenic systems should be checked carefully. Since the range of

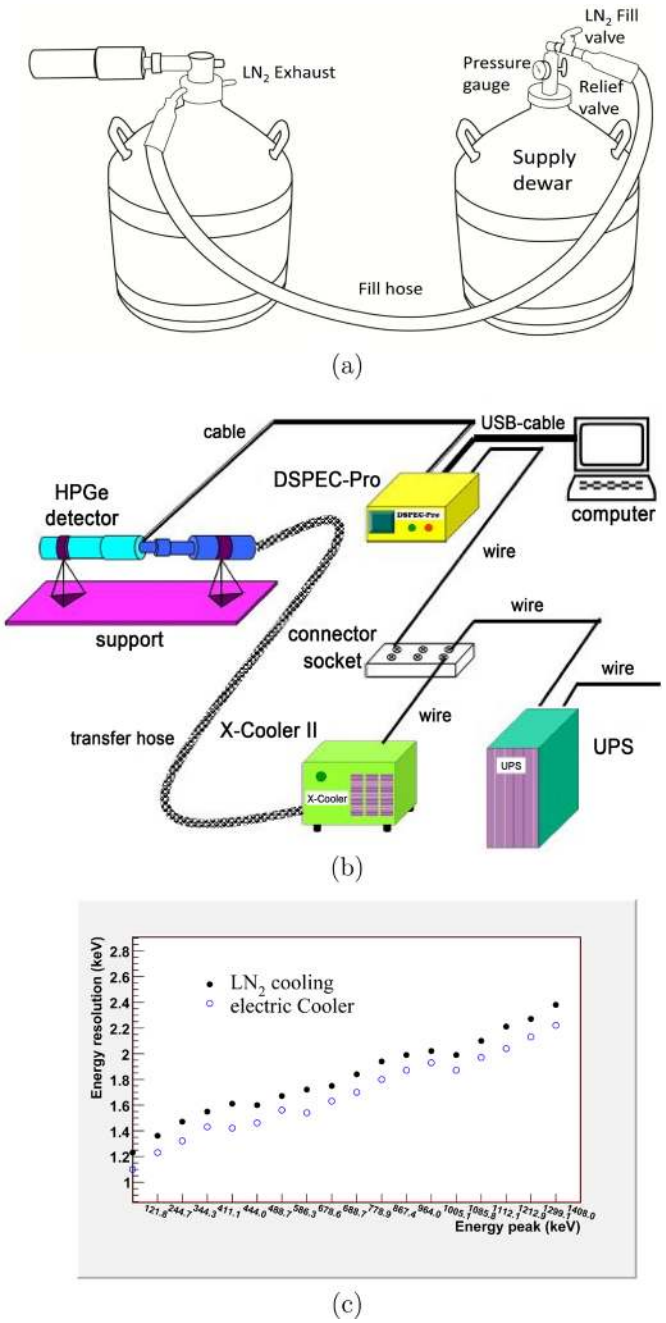

Figure 7. The HPGe detector cooled by two different refrigeration modes and the corresponding performance. (a) The LN_2 cooling case, the LN_2 is transfer using the self-pressuring system. (b) The electric cooler case. (c) The comparison of the detector resolutions to the characteristic lines of ^{152}Eu under LN_2 cooling method represent as dot and electric cooler case indicated as circle.

cooling temperature for electric cooler is from 85 to 105 K, that is a little bit higher than that for LN_2 (the boiling temperature for LN_2 is 77 K at standard temperature and pressure), it is believed that the resolution under LN_2 cooling condition would be better. A laboratory experiment was design and performed [21] to investigate the resolution under the two cryogenic conditions.

During the experiment, a point like radiation source of ^{152}Eu, whose main lines are from hundred keV to 1.4 MeV [22] [23], was placed along the cylindrical center axis of the germanium crystal, and about 1 cm far from the top of the germanium detector. A 1 cm foam plate was inserted between the source and the detector. The HPGe detector was calibrated by ^{137}Cs and ^{60}Co before experiment.

The experiment began with the electric cooler case, the design of the electric cooler can be found in **Figure 7(b)**. The data were collected after the HPGe exposed to radiation source from 9:00 Nov. 21, 2012 to 16:50 Nov. 23, 2012. In order to remove the background effect, 3 days' background data were taken before and after the ^{152}Eu nuclide measurement, separately.

After the above experiment, the PopTop capsule of the detector was removed from the cold head of the electric cooler, then connected with the cryostat, and put into a dewar filled with liquid nitrogen. After about 6 hours cooling, the germanium crystal was cold enough to apply the high voltage to bias the detector. The detector was calibrated using ^{137}Cs and ^{60}Co before ^{152}Eu measurement under LN_2 cooling condition. The radiation source experiment was performed from 17:00 Dec. 7, 2012 to 8:00 Dec. 10, 2012. Also the background data of about 3 days were taken before and after the measurement of ^{152}Eu under the LN_2 cooling, respectively.

The comparison of the detector resolutions to the characteristic lines of ^{152}Eu under different cooling methods are shown in **Figure 7(c)**. As described in Ref. [21], the shape of the lines are almost same, but the resolution of the germanium detector using the electric cooler is about 10% better than that using the LN_2 case. The noise level for both LN_2 and electric cooler is the same, about 10 keV.

The laboratory measurements indicate that the resolution of HPGe detector under the electric cooler is better than that using liquid nitrogen cooling. Therefore, the electric cooler is installed in the summer of 2013 to replaced the LN_2 cooling.

4.2. Alternating Moving Shielding

Since the HPGe detector is located near the beam pipes of collider, radiation background due to beam loss is extremely high [24] [25]. In order to protect the HPGe detector from radiation damage, a special design of radiation protect is indispensable [24]. In actual running period, the detector is surrounded by 5 cm of lead on all the sides, by 1.5 cm of iron below, and by 5 cm of lead above. Moreover, it is also shielded by 10 cm of paraffin on all sides. Since the main radiation background comes from the beam direction, an additional 11 cm of lead is installed in the beam direction [10].

However, even with the above protections, the radiation background along the beam direction seems still high. For improvement, an alternating moving shielding device was designed for further protection. As shown in **Figure 8(a)**, two movable stages with 10 cm thickness of leads were fixed on an aluminum electric push rod, they can move in the range of 350 mm and its movement speed of 8 mm per second. The electric push rod was installed between the HPGe detector and the short vacuum chamber as shown in **Figure 5**. If need, these leads can move into the beam direction to shield the high

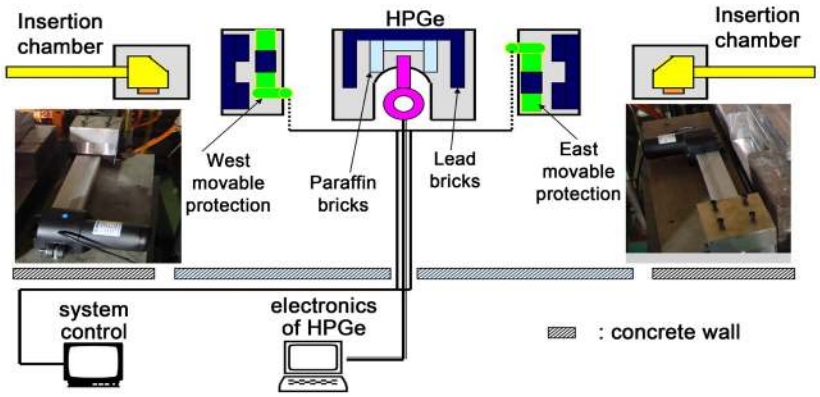

(a)

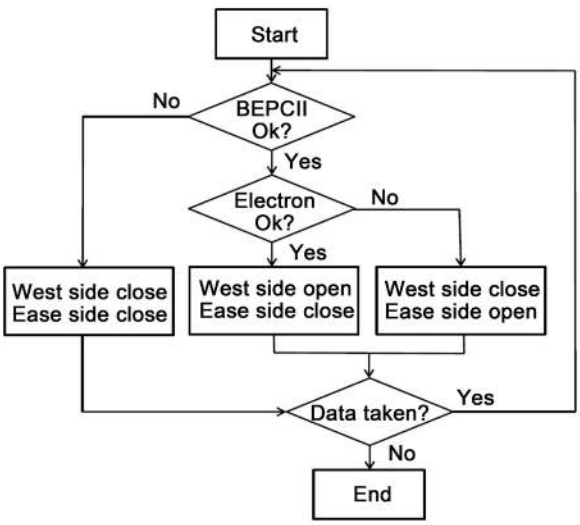

(b)

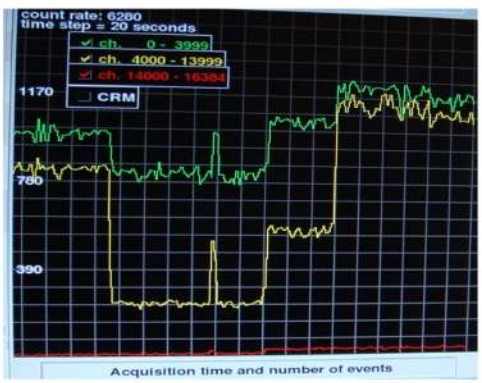

(c)

Figure 8. The movable shielding. (a) A sketch of the movable shielding, which is installed between the HPGe detector and laser insertion chamber. (b) The flow chart of the movable protection working principle. (c) The improvement of the signal to background ratio using moving shielding. The green line presents the low energy background, the yellow line illustrates the (S + B). when the laser is turned off, the yellow line illustrates the pure background (B). The left part shows the case when the moving shielding is used, the S/B is about 3.92, without out moving shielding case shown in the right part, the S/B is about 2.08.

energy photons coming from the other direction. For example, assuming the energy of positron beam need to be measured, the movable lead at the positron side (east side) will move out from the beam direction, and the backscattered photon will enter into the sensitive volume of germanium detector for measurement. However the electron side (west side) movable lead will move into the direction to shield the radiation photons from the electron beam. The working flow chart of the movable shielding is shown in **Figure 8(b)**.

The improvement due to the shielding device for the ratio of signal to background (RSB) is shown in **Figure 8(c)**, which can be seen that almost one time augment of RSB is obtained by using the moving shielding device.

5. Data Acquisition and Processing

5.1. Data Acquisition System

The relation between the maximal energy of the scattered photon $\omega_{\max}$ and the beam energy ε is provided by Comptom scattering theory [26] [27], that is

$$\omega_{\max} = \frac{\varepsilon^2}{\varepsilon + m_e^2/4\omega_0}, \tag{2}$$

where ω_0 is the energy of initial photon emitted by laser. The energy $\omega_{\max}$ can be determined through the detection of scattered photons by HPGe detector. Then the beam energy can be deduced from above formula,

$$\varepsilon = \frac{\omega_{\max}}{2}\left[1+\sqrt{1+\frac{m_e^2}{\omega_0\omega_{\max}}}\right]. \tag{3}$$

The actual data acquisition system is executed automatically, which is controlled by software. The layout of data acquisition system of BEMS is shown in **Figure 9(a)**. The working procedure is as follows: Firstly, some requirements (such as data taken time, data type, or energy difference range) are input as parameters into the software, then the software visits the BEPCII database and get the status parameters of the accelerator, such as beam currents, lifetime, energy value and so on. Then the HPGe detector begins to take data. Every few seconds, the HPGe detector measurements are stored and the detector counting rate is calculated. The mirrors are adjusted automatically to a position with a maximal photon/beam interaction using the feedback from the detector counting rate.

If the status of the accelerator is changed sufficiently, such as energy drift or beam loss, the current spectrum is saved and named as the end time of data taken, the next spectrum acquisition cycle at the same beam side is launched. Simultaneously, another program processes the saved data, calibrates the energy scale, finds the Compton edge, and calculates the beam energy. Then the value of beam energy is written into the BEPC-II database.

The measurement will switch to the other side of the beam when the requested data acquisition time has finished or the status of measurement beam does not satisfy the requirement. The rotary stage will turn a certain degree and direct the laser into the

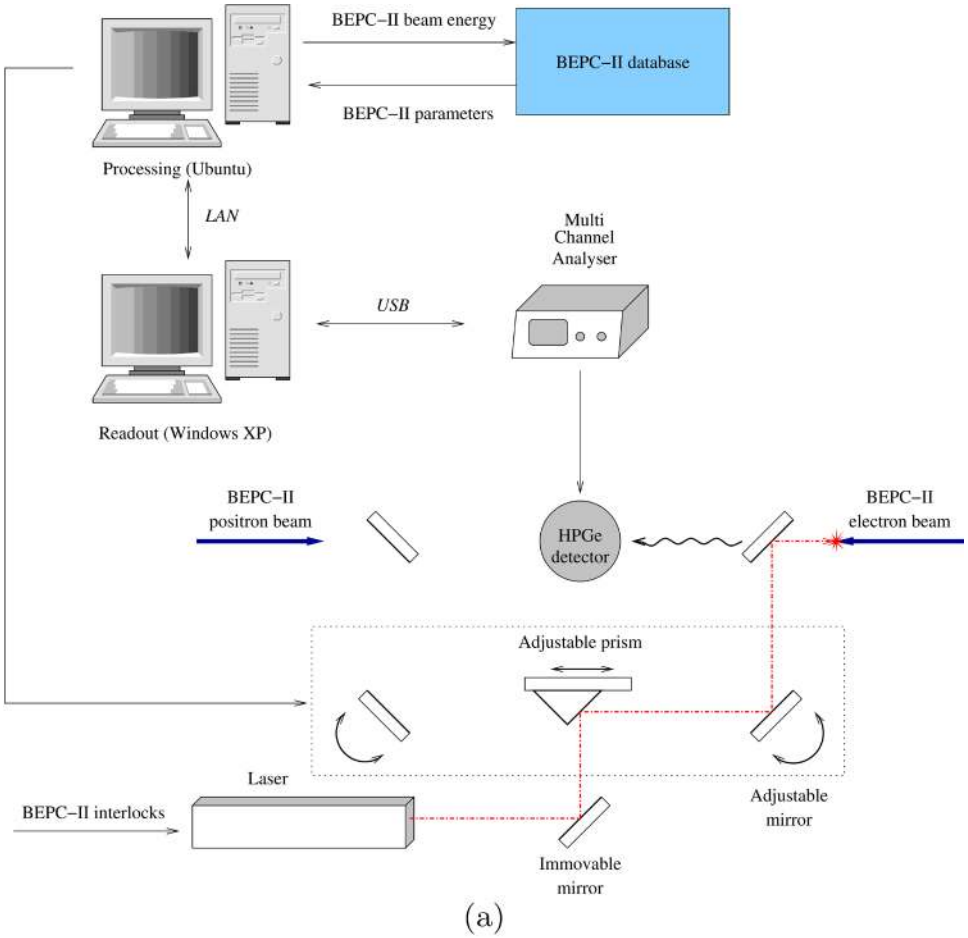

Figure 9. (a) Layout of the data acquisition system before upgrade, now the moving prism has been replaced by rotary stage. (b) The improved response function of the HPGe detector.

other side of the vacuum chamber for collision. The movable shielding leads as described in section 4.2 will move in or out the beam direction according to the requirement. All these adjustments are operated automatically.

5.2. Calibration Improvement

The kernel of the data acquisition system lies in the data processing, which is composed of three parts, that is calibration of energy scale, Compton edge fitting, and determination of beam energy. The improvement mainly consists in the response function and calibration source.

5.2.1. Response Function and Edge Fitting

The goal of calibration is to obtain the coefficients needed for conversion of detector's ADC counts into corresponding energy deposition, measured in units of keV as well as determination of the detector's response function parameters. The following response function was used:

$$f\left(x,x_0,\sigma,\xi\right)=\frac{N}{\sqrt{2\pi}\sigma}\cdot\begin{cases}\exp\left\{-\dfrac{\left(x-x_0\right)^2}{2\sigma^2}\right\}, & x>x_0-\xi\cdot\sigma\\ \exp\left\{\dfrac{\xi^2}{2}+\dfrac{\left(x-x_0\right)^2}{2\sigma^2}\right\}, & x<x_0-\xi\cdot\sigma,\end{cases}\tag{4}$$

$$\frac{1}{N}=\int_{-\infty}^{+\infty}f\left(x,x_0,\sigma,\xi\right)\mathrm{d}x=\frac{1}{2}\mathrm{erfc}\left(-\frac{\xi}{\sqrt{2}}\right)+\frac{1}{\sqrt{2\pi}\xi}\exp\left(-\frac{\xi^2}{2}\right).\tag{5}$$

where N is amplitude with normalization, x_0 is the position of peak, ξ is an asymmetry parameter, and σ is the full width of Gaussian distribution at half maximum divided by 2.36. The edge of backscattered photons spectrum is fitted by the function:

$$S_2\left(x,x_0,\sigma,\sigma_s,\xi\right)=\int_x^{+\infty}S_1\left(y,x_0,\sigma,\sigma_s,\xi\right)\mathrm{d}y+p_1\left(x\right).\tag{6}$$

Here $p_1\left(x\right)$ takes into account background contribution and S_1 is a convolution of the step function $\theta\left(x_0-x\right)$:

$$\theta\left(x_0-x\right)=\begin{cases}1, & x<x_0\\ 0, & x>x_0,\end{cases}\tag{7}$$

which describes the "pure" edge shape with the response function of HPGe detector (4) and Gaussian:

$$g\left(x,x_0,\sigma_s\right)=\frac{1}{\sqrt{2\pi}\sigma_s}\exp\left\{-\frac{\left(x-x_0\right)^2}{2\sigma_s^2}\right\},\tag{8}$$

which takes into account the energy spread of backscattered photons due to energy distribution of the collider beam.

$$\begin{aligned}S_1\left(x,x_0,\sigma,\sigma_s,\xi\right)=\frac{N}{2\sqrt{2\pi}}\times\Bigg[&\frac{1}{\sigma}\exp\left(\frac{\xi^2}{2}\left(1+\frac{\sigma_s^2}{\sigma^2}\right)+\frac{\xi x}{\sigma}\right)\cdot\mathrm{erfc}\left(\frac{\xi\left(\sigma^2+\sigma_s^2\right)+x\sigma}{\sqrt{2}\sigma\sigma_s}\right)\\&+\frac{1}{\sqrt{\sigma^2+\sigma_s^2}}\exp\left(-\frac{x^2}{2\left(\sigma^2+\sigma_s^2\right)}\right)\cdot\mathrm{erfc}\left(-\frac{\xi\left(\sigma^2+\sigma_s^2\right)+x\sigma}{\sqrt{2\left(\sigma^2+\sigma_s^2\right)}\sigma_s}\right)\Bigg].\end{aligned}\tag{9}$$

The edge position $\omega_{\max} \equiv x_0$, σ_s and coefficients of the first-order polynomial $p_1(x)$ are the free parameters of fit. Using the $\omega_{\max}$ value obtained from fit, the average beam energy ε_{nip} ("*nip*" denotes the north interaction region) in the $e-\gamma$ interaction region is calculated according to formula (3). Taking into account the energy losses due to synchrotron radiation, the beam energy in the south interaction point (*sip*) is obtained as

$$\varepsilon_{sip}(\mathrm{MeV}) = \varepsilon_{nip}(\mathrm{MeV}) + 4.75\times10^{-3}\times\left(0.001\times\varepsilon_{nip}(\mathrm{MeV})\right)^4. \tag{10}$$

The above response function, formula (4), can not describe the distribution of of the characteristic peak of radiation source precisely, therefore a wider Gaussian is introduced to improve the description of the left part of the peak. The improved response function, as shown in **Figure 9(b)**, becomes complex as follows:

$$f(x) = A\cdot\begin{cases} \exp\left[-\dfrac{(x-x_0)^2}{2\sigma^2}\right], & 0 < x-x_0 < +\infty, \\ C+(1-C)\exp\left[-\dfrac{(x-x_0)^2}{2(K_0\sigma)^2}\right], & -K_0\xi\sigma < x-x_0 \le 0, \\ C+(1-C)\exp\left[\xi\left(\dfrac{(x-x_0)}{2(K_0\sigma)}+\dfrac{\xi}{2}\right)\right], & -\infty < x-x_0 \le -K_0\xi\sigma, \end{cases} \tag{11}$$

where A is amplitude with normalization, x_0 is the position of peak. σ is the deviation of gaussian distribution from x_0 to the right. $K_0\sigma$ is the deviation of the other gaussian distribution from $x_0-\xi(K_0\sigma)$ to x_0, and $x_0-\xi(K_0\sigma)$ is the position where the exponential tail appears. C is responsible for the small angle Compton scattering of γ quanta in the passive material between the source and the detector. ξ is the asymmetry parameter.

The calibration procedure is the same as mentioned before. The parameters x_0, σ, K_0, ξ, C are determined when the calibration peaks are identified and fit.

After calibration, we need to measure the energy position of the sharp edge of the energy sprectrum of backscattered photons. The function to fit the edge was obtained in two steps. Firstly, we calculate the convolution of the response function with another gaussion, which is responsible for the energy spread in the beam:

$$\begin{aligned} S(x) = \frac{1}{2\sqrt{2\pi}}\Bigg\{ & \frac{1}{\sqrt{\sigma^2+\sigma_s^2}}\exp\left(\frac{-x^2}{2(\sigma^2+\sigma_s^2)}\right)\mathrm{erfc}\left(\frac{-x\sigma}{\sigma_s\sqrt{2(\sigma^2+\sigma_s^2)}}\right)+\frac{C}{\sigma}\mathrm{erfc}\left(\frac{x}{\sqrt{2}\sigma_s}\right) \\ & +\frac{(1-C)K_0}{\sqrt{\sigma_m^2+\sigma_s^2}}\exp\left(\frac{-x^2}{2(\sigma_m^2+\sigma_s^2)}\right)\left(\mathrm{erfc}\left(\frac{x\sigma_m}{\sigma_s\sqrt{2(\sigma_m^2+\sigma_s^2)}}\right)-\mathrm{erfc}\left(\frac{K_1(\sigma_m^2+\sigma_s^2)+x\sigma_m}{\sigma_s\sqrt{2(\sigma_m^2+\sigma_s^2)}}\right)\right) \\ & +\frac{1-C}{\sigma}\exp\left(\frac{K_1^2}{2}\left(1+\frac{\sigma_s^2}{\sigma_m^2}\right)+K_1\frac{x}{\sigma_m}\right)\mathrm{erfc}\left(\frac{K_1(\sigma_m^2+\sigma_s^2)+x\sigma m}{\sqrt{2}\sigma_s\sigma_m}\right)\Bigg\}, \end{aligned} \tag{12}$$

here x means $x-x_0$, the σ_s is responsible for the beam energy spread, and

$\sigma_m = K_0\sigma$. Then the Compton edge is fitted with:

$$S_1(x, x_0, \sigma, K_0, K_1, C, \sigma_s) = B + \int_x^{+\infty} S(y, x_0, \sigma, K_0, K_1, C, \sigma_s)\mathrm{d}y. \quad (13)$$

where B is the background. During edge fitting, the parameters σ, K_0, ξ are fixed to the values obtained from the calibration. From the fitting results, one can get the beam energy, energy spread, and background.

5.2.2. Calibration Source Upgrade

The energy to be measured at BEPC-II ranges from 1 to 2 GeV, the corresponding energy range of the backscattered photons is from 2 to 6 MeV. The calibration sources used from the very beginning of BEMS commissioning are as follows:

- ^{137}Cs: $E_\gamma = 661.657 \pm 0.003$ keV
- ^{60}Co: $E_\gamma = 1173.228 \pm 0.003$ keV
- ^{60}Co: $E_\gamma = 1332.492 \pm 0.004$ keV
- ^{16}O*: $E_\gamma = 6129.266 \pm 0.054$ keV

However, between 2 and 6 MeV, there is no source for calibration. To remedy such a defect, besides radiation sources listed above, a precise pulse generator is adopted for detailed calibration purposes.

The ORTEC® DSPEC Pro™ MCA has a ±250 ppm declared integral non-linearity (in 99.5% of scale). A precision pulse generator (BNC model PB-5) is declared by manufacturer to have ±15 ppm integral non-linearity and ±10 ppm amplitude jitter. The PB-5 outlet is connected to HPGe preamp inlet to provide a set of discrete pulse amplitudes, forming a corresponding set of peaks in the measured spectrum. The PB-5 pulse shaping parameters were selected as follows:

- Attenuation: 10,
- Pulse rise time: 50 ns (minimum),
- Pulse width: 14 μs (pulse top: flat),
- Pulse fall time: 500 μ,
- Pulse amplitudes: 0.75, 1.20, 1.40, 1.65, 1.75, 2.10, 2.50, 2.90, 3.40, 4.00, 4.50, 5.00, 5.40, 6.10, 6.50, 7.00, 8.50, 9.00, 10.0 V, forming 19 calibration peaks;
- Pulse repetition rate: 20 - 50 Hz.

Switching between different amplitudes listed above occurs randomly in time via a simple computer script.

To test the calibration effect, two reference lines from [^{232}Pu ^{13}C] gamma were used. α-decay of ^{232}Pu provides the reaction:

$$\alpha + {}^{13}\mathrm{C} \to n + {}^{16}\mathrm{O}^*. \quad (14)$$

An exited oxygen nuclei emits γ-rays with energy of 6129.266 ± 0.054 keV [28]. The p-type HPGe detector used at BEPC-II is shielded from neutrons, emitted in the reaction (14), by about 10 cm of paraffin. The presence of these neutrons leads to the reaction:

$$n + p \to d + \gamma, \quad (15)$$

from which we can observe the 2223 keV γ-rays as a by-product of such a configuration. This energy can be found in Refs. [29] [30].

Table 1 lists the results of measured energies from γ-ray and pulse generator. The comparison confirms the reliability of pulse calibration.

6. Laser Interlock System

Laser is invisible, dangerous to person who works in the corridor or tunnel near the NIP of BEPC-II. Laser interlock system is a good way to protect people from the laser damage. Figure 10 shows the schematic diagram of interlock of BEMS. Only when people evacuate from the BEPC-II storage ring, and the tunnel door is closed, can the BEMS laser be activated, and an indicator light will be turned on. After the shutter control is switched on, the laser will be emitted.

As mentioned before, the laser is located in the corridor. It will be dangerous to the BEMS staff who enter the corridor, therefore the door of corridor is interlocked with the laser. When the corridor door is open, the laser output will be terminated automatically.

When the moving prism was replaced by the rotary platform, the beam measurement switch between electron and positron became dangerous, because the laser would rotate 180 degrees according to the platform rotary. Once laser meets the flammable material, it is likely to cause fire. Therefore, the status of BEMS has to be interlocked with laser. When the measured beam needs to be switched, the laser will be turned off before the rotary platform is rotating.

Table 1. The comparison of measured energies from γ-ray and pulse generator.

Energy	γ-ray	Pulse generator	Reference
6129 keV	6129.451 ± 0.064 keV	6129.208 ± 0.062 keV	6129.266 ± 0.054 keV
2223 keV	2223.144 ± 0.272 keV	2223.149 ± 0.022 keV	2223.24835 ± 0.00008 keV

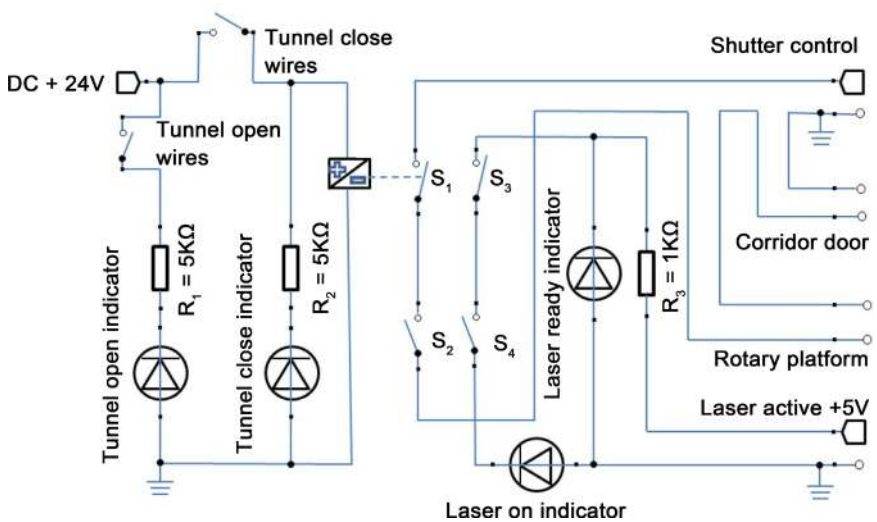

Figure 10. Schematic diagram of the interlock system of BEMS.

A main switch was installed near the corridor door. This switch is disconnect during the BEMS instruments test and adjust in the corridor. Only when all operations are performed, will the main switch be turned on, will the laser be operate.

The detailed interlock information is shown in Figure 10.

7. Upgrade Effect

The effect of upgrade BEMS was checked during the Y(2235) data taken in April 2015. Figure 11(a) and Figure 11(b) show the measured Compton edge of scattered photons energy spectrum with upgraded components for electron and positron separately. It is clear that twelve minutes' data collection, the compton edge is very sharp. The fit results are listed in Table 2. The measurement precision of beam energy is about 6.5×10^{-5}, the energy spread is better than 15%. A beam energy measurement was built at VEEP-2000 in 2014 [31]. Using the same data taking time, our measurement precision is better than that of VEEP-2000.

8. Summary

BEMS has greatly increased the measurement capacity for both BEPC-II accelerator and BES-III detector, and has become an indispensable part of them. Many technique details were provided for clearly understanding the working process of the whole system; especially the upgrade improvement was described in detail.

Summarized in Table 3 are the main upgraded components of BEMS during the past several years. More powerful laser, higher transmission rate of ZnSe lenses and viewports will intensify the number of photons colliding with beams, lessen the data taking time for measurement at the same accuracy. Because of the usage of an X-cooler II instead of LN_2, the LN_2 refilling time is no longer needed, and such time is saved for the

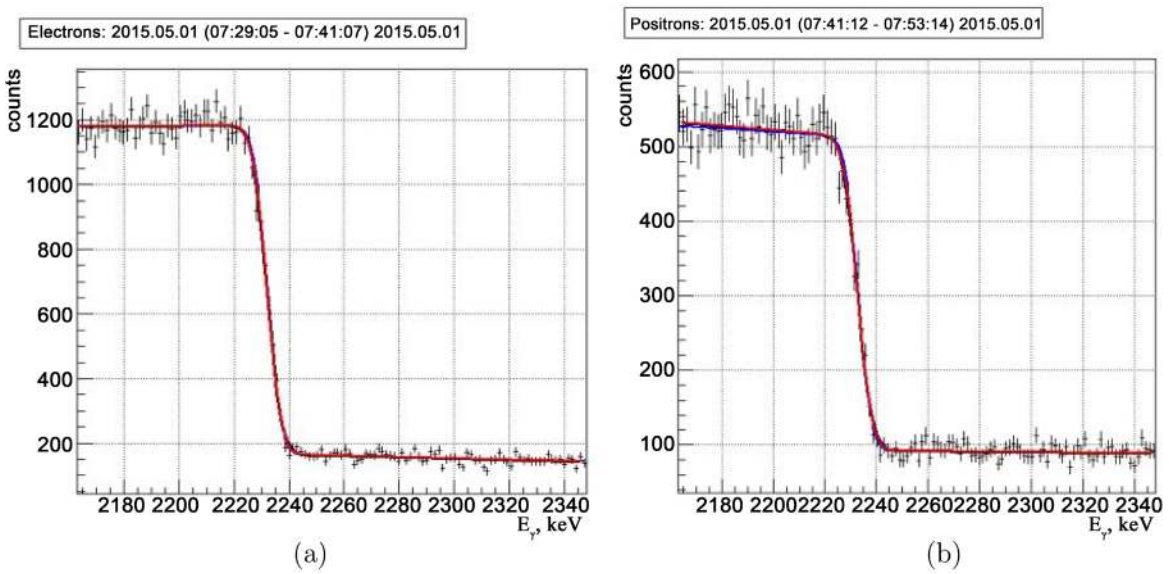

Figure 11. The measured edge of the scattering photons energy spectrum. The line is the fit result. (a) Electron case, (b) Positron case.

Table 2. The typical values of beam energy and energy spread after BEMS upgrade.

	Positron	Electron
Energy (MeV)	1117.134 ± 0.071	1116.763 ± 0.039
Energy spread (keV)	726.9 ± 102.6	741.1 ± 50.6

Table 3. The upgradation chronicle of BEMS.

Previous system	Upgraded system	Upgrade time	Improvement
Focus lenses ZnSe	new focus lenses	2011.4	laser transmission rate rise to 98%
No moving shielding	10 cm moving shielding	2011.9	higher signal background ratio
No interlock	USB interface relay	2012.3	protect staff from laser
Moving prism	rotary platform	2012.3	more durable
LN_2 cooling	electric cooler cooling	2013.8	LN_2 refill time is saved
GaAs viewport	ZnSe viewport	2014.8	laser transmission rate rise to 76%
Laser with line 10P42	Laser with line 10P02	2014.12	laser power rise to 50 W

data collection. The new calibration response function for the HPGe detector and fitting function for the energy spectrum will help to get more precise beam energy.

After the above improvement, BEMS is more efficient, more BES-III running time is spent on data collection, and the time required to determine the beam energy is about one fourth of that used before improvement. More precise energy measurement results are expected for the forthcoming BES-III analysis.

Acknowledgements

Authors would like to acknowledge great supports and helps from colleagues of both BESIII detector and BEPCII accelerator in the construction and improvement of BEMS. Special thanks are due to Prof. Wei-Guo Li for the clear expression of the relevant physical thoughts and inspection of the energy shift issue of BEMS.

Fund

This study is supported in part by National Natural Science Foundation of China (NSFC) under contracts Nos.: 11375206, 10775142, 10825524, 11125525, 11235011; the Ministry of Science and Technology of China under Contract Nos.: 2015CB856700, 2015CB856705; State key laboratory of particle and detection and electronics; and the CAS Center for Excellence in Particle Physics (CCEPP); the RFBR grant No 14-02-00129-a; U.S. Department of Energy under Contracts No. DE-FG02-04ER41291, No. DE-FG02-05ER41374, No. DE-FG02-94ER40823, No. DESC0010118; U.S. National Science Foundation; part of this work related to the design of ZnSe viewports is supported by the Russian Science Foundation (project No 14-50-00080).

References

[1] Wang, J.Q., *et al.* (2010) Status and Performance of BEPCII. *Proceedings of International*

Particle Accelerator Conference (*IPAC*'10), Kyoto, 23-28 May 2010, 2359-2361.

[2] Preliminary Design Report of Accelerator BEPC (2003) Second Version. (In Chinese) http://acc-center.ihep.ac.cn/bepcii/bepcii.htm

[3] Ablikim, M., *et al.* (2010) Design and Construction of the BESIII Detector. *Nuclear Instruments and Methods in Physics Research*, **614**, 345-399. http://dx.doi.org/10.1016/j.nima.2009.12.050

[4] Chao, K.-T. and Wang, Y.-F. (2009) Physics at BESIII. *International Journal of Modern Physics A* (Suppl. Issue 1), **24**, iii-xix. http://www.worldscientific.com/doi/pdf/10.1142/S0217751X09046400

[5] Fu, C.-D. and Mo, X.-H. (2008) Significance of Absolute Energy Scale for Physics at BESIII. *Chinese Physics C*, **32**, 776-780. http://dx.doi.org/10.1088/1674-1137/32/10/002

[6] Mo, X.-H. (2007) Study of High Precision τ Mass Measurement at BESIII. *Nuclear Physics B—Proceedings Supplements*, **169**, 132-139. http://dx.doi.org/10.1016/j.nuclphysbps.2007.02.107

[7] Wang, Y.-K., Mo, X.-H., Yuan, C.-Z. and Liu, J.P. (2007) Optimization of the Data Taking Strategy for a High Precision τ Mass Measurement. *Nuclear Instruments and Methods in Physics Research*, **583**, 479-484. http://dx.doi.org/10.1016/j.nima.2007.09.026

[8] Achasov, M.N., *et al.* (2009) Energy Determination at BEPC-II. *Nuclear Physics B—Proceedings Supplements*, **189**, 366-370. http://dx.doi.org/10.1016/j.nuclphysbps.2009.03.059

[9] Mo, X.-H., *et al.* (2010) Beam Energy Measurement System at BEPC II. *Chinese Physics C*, **34**, 912-917. http://dx.doi.org/10.1088/1674-1137/34/6/050

[10] Abakumova, E.V., *et al.* (2011) The Beam Energy Measurement System for the Beijing Electron-Positron Collider. *Nuclear Instruments and Methods in Physics Research Section A*, **659**, 21-29. http://dx.doi.org/10.1016/j.nima.2011.08.050

[11] Zhang, J.Y., *et al.* (2012) The Beam Energy Measurement System for the Beijing Electron-Positron Collider. *Nuclear Physics B—Proceedings Supplements*, **225-227**, 309-314. http://dx.doi.org/10.1016/j.nuclphysbps.2012.02.064

[12] Ablikim, M., *et al.* (2014) Precision Measurement of the Mass of the τ Lepton. *Physical Review D*, **90**, Article ID: 012001.

[13] Mo, X.-H., *et al.* (2008) Working principles of the energy measurement system at BEPCII. *Chinese Physics C*, **32**, 995-1002. http://dx.doi.org/10.1088/1674-1137/32/12/011

[14] Patel, C.K.N. (1964) Continuous-Wave Laser Action on Vibrational-Rotational Transitions of CO_2. *Physical Review*, **136**, 1187-1193. http://dx.doi.org/10.1103/PhysRev.136.A1187

[15] Abakumova, E.V., Achasov, M.N., Krasnov, A.A., *et al.* (2015) The System for Delivery of IR Laser Radiaton into High Vacuum. *Journal of Instrumentation*, **10**, Article ID: T09001. http://dx.doi.org/10.1088/1748-0221/10/09/T09001

[16] Abakumova, E., *et al.* (2012) Vacuum Chamber for the Measurement System of the Beam Energy. *Physics Procedia*, **32**, 753-756. http://dx.doi.org/10.1016/j.phpro.2012.03.630

[17] Achasova, M.N. and Yu, N. Muchnoia. arXiv:1404.2094v1

[18] Knoll, G.F. (1979) Radiaiton of Detectrion and Measurement. John Wiley & Sons, New York.

[19] User's Manual. X-Cooler II Mechanical Cooler for HPGe Detector, ORTEC.

[20] Gin, D., *et al.* ITER High Resolution Gamma Spectrometry. ITR/P5-39. http://www-naweb.iaea.org/napc/physics/FEC/FEC2012/papers/423_ITRP539.pdf

[21] Zhang, J., Cai, X. and Mo, X. (2013) On Two Cryogenic Systems of High Purity Germanium Detector. *Detection*, **1**, 13-20. http://dx.doi.org/10.4236/detection.2013.12003

[22] Grigorescu, E.L., *et al.* (2002) Standardization of ^{152}Eu. *Applied Radiation and Isotopes*, **56**, 435-439. http://dx.doi.org/10.1016/S0969-8043(01)00227-5

[23] Yang, Q.L., *et al.* (2012) Preparation of Standard Radioactive Solution of ^{152}Eu. *Journal of Nuclear and Radiochemistry*, **34**, 223-228.

[24] Mo, X.-H., Zhang, J.-Y., Zhang, Q.-J., *et al.* (2011) Study of Radiation Background at the North Crossing Point of the BEPC II in Collision Mode. *Chinese Physics C*, **35**, 642-655. http://dx.doi.org/10.1088/1674-1137/35/7/009

[25] Mo, X.-H., Zhang, J.-Y. and Zhang, T.-B. (2009) Measurement of Radiation Dose at the North Interaction Point of BEPC II. *Chinese Physics C*, **33**, 914-921. http://dx.doi.org/10.1088/1674-1137/33/10/017

[26] Achasov, M.N., *et al.* (2008) BINPP Reprint 2008-4. ArXiv:0804.0159

[27] Mo, X. (2014) Uncertainty of the Beam Energy Measurement in the e^+e^- Collision Using Compton Backscattering. *Chinese Physics C*, **38**, Article ID: 106203. http://dx.doi.org/10.1088/1674-1137/38/10/106203

[28] Alkemade, P.F.A., Alderliesten, C., De Wit, P. and Van der Leun, C. (1982) The Energy of the 6.13 MEV γ-Transition in ^{16}O Related to the Gold Standard. *Nuclear Instruments and Methods in Physics Research*, **197**, 383-390. http://dx.doi.org/10.1016/0167-5087(82)90332-5

[29] Kessler Jr., E.G., Dewey, M.S., Deslattes, R.D., Henins, A., Borner, H.G., Jentschel, M., Doll, C. and Lehmann, H. (1999) The Deuteron Binding Energy and the Neutron Mass. *Physics Letters A*, **255**, 221-229. http://dx.doi.org/10.1016/S0375-9601(99)00078-X

[30] Database of Prompt Gamma Rays from Slow Neutron Capture for Elemental Analysis (2007) STI/PUB/1263. 251 p.

[31] Abakumova, E.V., Achasov, M.N., Berkaeva, D.E., *et al.* (2014) A System of Beam Energy Measurement Based on the Compton Backscattered Laser Photons for the VEPP-2000 Electron-Positron Collider. *Nuclear Instruments and Methods in Physics Research*, **774**, 35-40. http://dx.doi.org/10.1016/j.nima.2014.01.020